Calcium optical frequency standard with ultracold atoms: Approaching 10^{-15} relative uncertainty

Carsten Degenhardt,* Hardo Stoehr,† Christian Lisdat,‡ Guido Wilpers,§ Harald Schnatz, Burghard Lipphardt, Tatiana Nazarova, Paul-Eric Pottie,‖ Uwe Sterr, Jürgen Helmcke, and Fritz Riehle
Physikalisch-Technische Bundesanstalt, Bundesallee 100, 38116 Braunschweig, Germany
(Received 9 March 2005; published 21 December 2005)

An optical frequency standard based on an ensemble of neutral calcium atoms laser-cooled to 12 μK has been realized. By using ultracold atoms, one major previous source of uncertainty, the residual Doppler effect, was reduced. We show that cold collisions contribute a negligible amount to the uncertainty. The influence of a temporal evolution of the phase of the laser pulses used to interrogate the clock transition was measured and corrected for. The frequency of the clock transition at 657 nm was referenced to the caesium fountain clock of PTB utilizing a femtosecond comb generator with a fractional uncertainty of 1.2×10^{-14}. The transition frequency was determined to be (455 986 240 494 144±5.3) Hz, making the calcium clock transition one of the most accurately known optical transitions. A frequency stability of 3×10^{-15} at 100 s averaging time was achieved and the noise contributions that limit to the observed stability were analyzed in detail. Additionally, the natural linewidth of the clock transition has been determined.

DOI: 10.1103/PhysRevA.72.062111 PACS number(s): 06.30.Ft, 42.62.Eh, 42.62.Fi

I. INTRODUCTION

Improvements in optical frequency standards during the past ten years revealed their potential to compete with the primary standards for frequency and time, the Cs clocks. In this range of accuracy there are essentially two types, single-ion and neutral atom frequency standards. For the single ion standards exceptionally low relative accuracy levels of 10^{-18} are projected [1,2]. On the other hand, the restriction to one single atom limits the achievable stabilities to the lower 10^{-15} range in 1 s.

Neutral atom standards use ensembles of 10^6 to 10^8 laser cooled atoms. Due to the high number of atoms extremely low instabilities are projected that are two orders of magnitude lower than in the case of the single ion standards. As a drawback, interactions between the atoms of the ensemble could lead to parasitic frequency shifts. Nevertheless, relative accuracies in the 10^{-16} range are expected [3]. With the invention of optical frequency comb generators [4], a transfer of the accuracy to electronically accessible rf frequencies is possible, which can also be realized with a stability substantially higher than the best microwave oscillator flywheels. With these prospects optical frequency standards are candidates for the best clocks of the future. Neutral atoms as well as single ions have been successfully applied in time and length metrology. Absolute frequency measurements with relative frequency uncertainties on the level of 10^{-14} have been performed for neutral Ca and Sr atoms [3,5–7] and for Hg^+, In^+, Sr^+, and Yb^+ ions [5,8–10].

In this paper we present a detailed description of our most recent frequency measurement [3] of the 657 nm ^{40}Ca optical frequency standard (clock transition in Fig. 1). The fractional uncertainty achieved was 1.2×10^{-14}, representing one of the most accurate frequency measurements of a neutral atom transition to date. We describe investigations of the key physical and technical issues that limit the laser-cooled standard's performance and show how a modified apparatus could achieve fractional uncertainties of 10^{-15} or less. In order to have a consolidated picture we use and extend previously published results when necessary.

We will first describe the ways we prepare the ultra-cold atoms (Sec. II). In Sec. III we introduce the atom interfero-

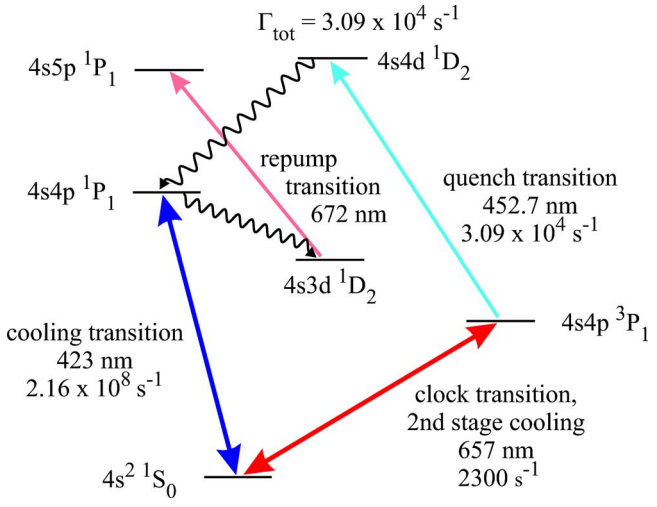

FIG. 1. (Color online) Partial energy level diagram of calcium. Only transitions relevant for the realization of the optical frequency standard are shown. The positions of the energy levels are not to scale.

*Present address: Philips Research Laboratories, 52066 Aachen, Germany.
†Present address: Institut für Biomedizinische Optik, Universität zu Lübeck, Peter-Monnik–Weg 4, 23562, Lübeck, Germany.
‡Present address: Institut für Quantenoptik, Universität Hannover, Welfengarten 1, 30167 Hannover, Germany.
§Present address: National Physical Laboratory, Teddington, Middlesex, TW11 0LW UK.
‖Present address: Laboratoire de Physique des Lasers, Institut Galilée—Université Paris 13, 99 avenue Jean-Baptiste Clément F-93430 Villetaneuse, France.

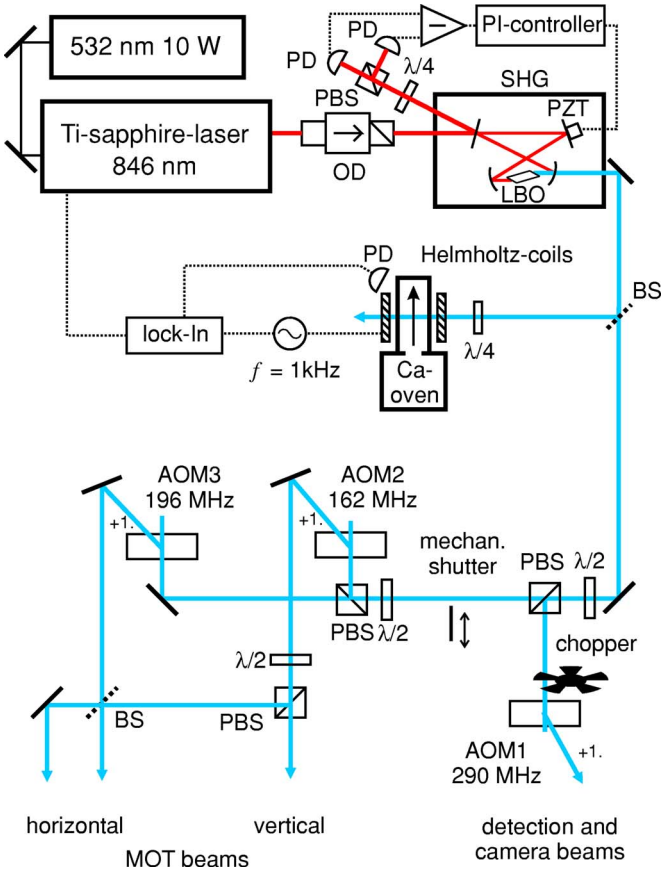

FIG. 2. (Color online) Laser system for cooling and detection at 423 nm. Upper right: Frequency doubler. Lower part: acousto-optical modulators used for switching and frequency offset. Center: Ca atomic beam for absolute frequency stabilization. OD: optical diode; PBS: polarizing beam splitter; BS: beam splitter; λ/2: λ/2 retarder; λ/4: λ/4 retarder; PD: photodiode; PZT: piezoelectric actuator.

metric method applied for probing the clock transition and absolute frequency stabilization. For the first time, the effect of reexcitation after spontaneous emission is taken into account. Comprehensive investigations of systematic uncertainties will be summarized in Sec. IV. The result of a frequency measurement utilizing a frequency comb generator and the Cs fountain of the PTB will be presented in Sec. V. Section VI deals with noise contributions to the signal and the achieved and predicted stability of the standard. A summary and a short outlook into the future of the calcium frequency standard will be given in Sec. VII.

II. PREPARATION OF THE ULTRACOLD ENSEMBLE

In the first cooling step Ca atoms are cooled on the allowed 423 nm transition $^1S_0$-$^1P_1$ and captured in a magneto-optical trap (MOT) consisting of a magnetic quadrupole field and three mutually perpendicular pairs of circularly polarized laser beams.

The cooling light for the MOT is produced by an all solid state laser system consisting of a frequency doubled titanium-sapphire laser (Fig. 2). The titanium-sapphire laser delivers 1.5 W of usable radiation at 846 nm. 85% of this radiation is coupled into a bow tie build-up cavity containing a Brewster-cut lithiumtriborate (LBO) crystal as the nonlinear medium. The finesse of the cavity is 250 and the total amount of usable output power at 423 nm is 670 mW.

The atoms are directly trapped from a thermal effusive beam of calcium atoms from an oven with a temperature of 900 K. The beam is directed towards the trap. The MOT center is shielded from the atomic beam by a beam-block to avoid collisions of the trapped atoms with the fast atomic beam. As no Zeeman slower is used, only a small fraction of the atoms from the Boltzmann velocity distribution ($\bar{v} \approx 700$ m/s) within the trap's capture velocity can be trapped. At a red detuning of the MOT beams of 94 MHz the capture velocity is about 30 m/s. To obtain an acceptable loading rate, first the oven was placed as close as possible to the trap center ($d \approx 15$ cm). Secondly, each of the horizontal trapping beams had a second laser beam superposed. These additional beams were detuned by 128 MHz to the red of the atomic line as to increase the capture velocity in the plane of the atomic beam [11]. We generated the bichromatic fields using the first diffraction orders of two switching acousto-optical modulators (AOM's) with different rf frequencies and overlaying the beams on a 50% beam splitter (Fig. 2).

During the cooling, there is a loss of atoms by a decay from the $^1P_1$ state to the $4s3d\ ^1D_2$ state, that occurs with a branching ratio of 10^{-5} [12]. From there, the excited atoms predominantly decay to the metastable $4s4p\ ^3P$ states and get lost from the trap before they decay into the ground state. This bypass was closed by exciting the atoms on the $4s3d\ ^1D_2$–$4s5p\ ^1P_1$ transition applying 2 mW of laser light at 672 nm (repump transition in Fig. 1). The light is generated by an extended cavity diode laser, which is stabilized to a tunable reference cavity.

From the $4s5p\ ^1P_1$ state, atoms then decay to the ground state and again take part in the cooling process. With the repumping laser the trap lifetime was increased from 20 ms to more than 300 ms and the number of trapped atoms was increased by a factor of five.

In this first step of the cooling process, the MOT at 423 nm is operated for 300 ms to 500 ms. About 10^8 atoms are stored at a temperature of 3 to 4 mK. This temperature is close to the Doppler limit of this transition, as no sub-Doppler mechanisms work due to the non-degenerate atomic ground state. Therefore, a second stage of cooling is applied using the forbidden 657 nm transition $^1S_0$-$^3P_1$. For efficient cooling the scattering rate is increased by quenching the upper state by excitation of the 453 nm transition from the metastable $^3P_1$ level to the $4s4d\ ^1D_2$ state [13]. Here, a stilbene 3 dye laser is used, which is pumped by a 3.5 W uv argon-ion laser. The dye laser is offset locked to an I_2 stabilized HeNe laser by means of a transfer cavity. The usable output power of the dye laser is about 80 mW. This MOT is operated for 20 ms to further cool the atoms down to 12 μK at a density of 4×10^{10} cm^{-3} and a total number $N = 3 \times 10^7$.

The velocity distribution of this ultracold ensemble was determined by measuring the Doppler broadening of the clock transition at 657 nm by excitation with a single running wave.

The density distribution and number of atoms of the trapped ensemble were determined from optical density mea-

surements utilizing the absorption by the ensemble of a laser beam resonant with the 423 nm transition.

Therefore, the atomic ensemble is well characterized in terms of atom number and density, as well as velocity and spatial distribution. These properties are of great importance for the realization and evaluation of an optical frequency standard.

III. PROBING THE CLOCK TRANSITION

For precision spectroscopy of the calcium clock transition with a resolution close to the natural linewidth, a highly stable spectroscopy laser and the utilization of atom interferometric methods in analogy to the separated field technique used for microwave transitions are necessary. Since the atoms are nearly at rest, the separation of the excitation regions can be realized with laser pulses applied in a time sequence. Furthermore, to probe the undisturbed clock transition all spurious external fields must be avoided. As the coils for the quadrupole and bias magnetic fields are inside the vacuum chamber to prevent eddy currents, the magnetic fields can be switched within 200 μs. All laser beams at the trap apparatus are switched with AOM's and additional mechanical shutters [14]. A time sequence with subsequent trapping and cooling ($\approx$500 ms), atom interferometry (40 μs up to 2 ms) and detection (1 ms) was applied for all measurements as well as during the operation of the optical frequency standard.

A. Spectroscopy laser

The diode laser system used for the spectroscopy and cooling at 657 nm consists of one master diode laser which injection locks four slave diode lasers (Fig. 3). The master laser is realized as an extended cavity laser in Littman configuration. The output radiation of the laser is stabilized with respect to an ultra-stable high finesse resonator by the Pound-Drever-Hall technique [15]. An AOM between the master laser and the resonator allows for frequency tuning. The 10 cm long resonator is made from ultralow expansion glass (ULE) with optically contacted supermirrors. The finesse is 80 000 with a linewidth of 18 kHz. The resonator is installed in an ultra-high vacuum environment with an active temperature stabilization. The whole system is suspended on springs inside an acoustically isolated housing to minimize the influence of mechanical vibrations. The linewidth of the laser system of around one Hertz was determined by recording the beat between two identical but independent systems [3].

Since the master laser is located in a quiet laboratory room, a 30 m long single mode polarization maintaining optical fiber is used to transmit the light to the laboratory with the calcium MOT. An interferometric technique is used to cancel frequency noise due to mechanical influences on the fiber [16].

The light of the master laser is used to injection lock slave laser 1 (Fig. 3). Most of the light of slave laser 1 is coupled into a fiber to the femtosecond comb generator located in another building. The rest of the light is used to injection

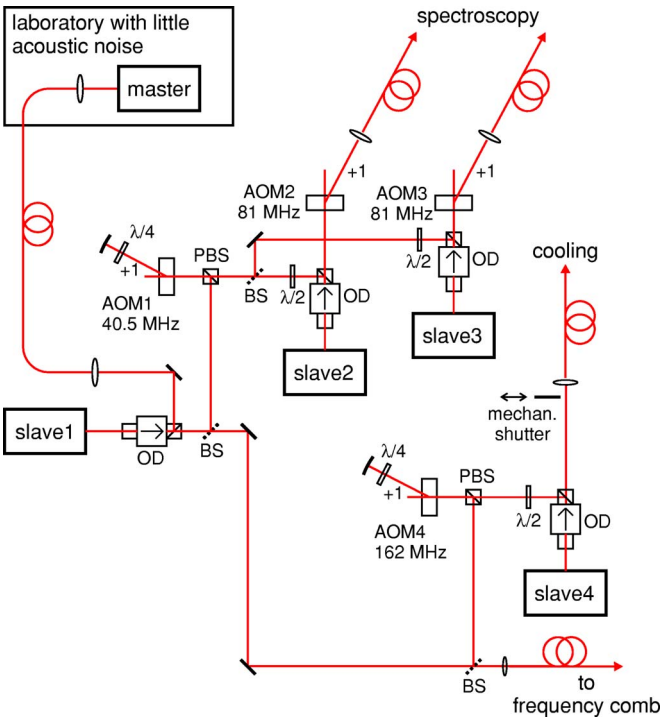

FIG. 3. (Color online) Laser system for cooling and spectroscopy at 657 nm. The light of the master diode laser is amplified with four slave diode lasers. The acousto-optical modulators are used for frequency offset and generation of the spectroscopy pulses. OD: optical diode; PBS: polarizing beam splitter; BS: beam splitter; $\lambda/2$: $\lambda/2$ retarder; $\lambda/4$: $\lambda/4$ retarder.

lock the three slave lasers 2–4. Slave laser 2 and slave laser 3 are used to generate the two counter-propagating spectroscopy beams. The acousto-optical modulator AOM1 is utilized to adjust the frequency and the phase of the light that injection locks the slave lasers 2 and 3. AOM2 and AOM3 serve as pure switching AOM's with a fixed operation frequency. AOM4 generates the sidebands necessary for the second stage cooling [13]. The cooling light at 657 nm is produced by slave laser 4. To block additionally the cooling light a mechanical shutter is used [14].

B. Atom-interferometric interrogation

Even at a temperature of 12 μK, the Doppler width of the intercombination line still amounts to a few hundred kHz. Therefore, a Doppler-free interrogation of the line is required. Here, a pulsed interrogation is used for precision spectroscopy that can be best described as an atom interferometer [17] that makes efficient use of an atomic ensemble. In saturation spectroscopy only a small part of the atoms from the Doppler broadened linewidth within the homogeneously broadened line contribute to the signal. Using atom interferometry in the time domain with a sequence of short laser pulses, the Fourier width of the pulses determines the homogeneous width. With ultracold Ca atoms this width can be larger than the Doppler width and therefore nearly all atoms contribute to the signal [18].

For the frequency standard, a frequency-dependent asymmetric four-pulse atom interferometer (AI) in the time do-

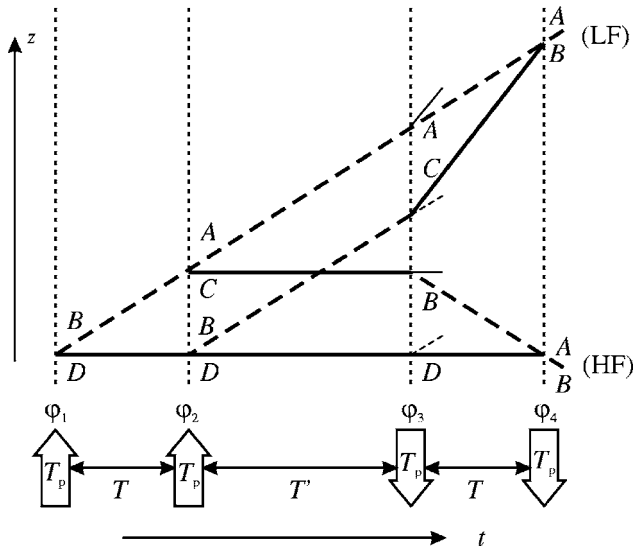

FIG. 4. Four pulse Ramsey-Bordé interferometer in the time domain. All beam splitter pulses are $\pi/2$ pulses. Full (dashed) lines indicate trajectories of atomic wave packets in the ground (excited) state leading to two trapezoidal interferometers that correspond to the high (HF) and low frequency (LF) recoil component. The letters indicate the complex transition amplitudes in each interaction as given in Eq. (4).

main is used (Fig. 4), where four rectangular pulses of collimated, running waves in two counter-propagating pairs are applied. The pulse width T_p of the pulses is set in combination with the irradiance I of the laser beams to provide an excitation probability of 0.5 for an atom in resonance, i.e., a Rabi-excitation angle of $\pi/2$.

In the language of atom interferometry the first interaction pulse splits the atomic wave packet into a superposition of ground and excited state wave packets like a beam splitter for atoms. At the same time the momentum of the interacting wave packet is changed by one photon recoil. The change in momentum, when a photon is absorbed or emitted, corresponds to a Doppler shift of $2\delta=23.1$ kHz with

$$\delta = \frac{h\nu_{\mathrm{Ca}}^2}{2M_{\mathrm{Ca}}c^2}, \tag{1}$$

where h denotes Planck's constant, M_{Ca} the Ca atomic mass and c the speed of light. Different paths develop that are redirected in the second and third interaction zone and overlayed again in the fourth one. As is shown in Fig. 4, two trapezoidal interferometer geometries exist with different numbers of photon recoils in the direction of the laser beams z. At the exits of the interferometer the probability p_e of detecting an atom in the excited state depends on the phase difference that the atomic wave functions have accumulated on their different paths.

This phase is a function of the detuning of the frequency of the exciting laser ν_L with respect to the transition frequency ν_{Ca}. We use the formalism developed in Ref. [19] to describe the oscillatory terms p_{HF} and p_{LF} of the interference pattern. In addition to Ref. [19], the incoherent background p_{inc} here also includes the possibility to reexcite atoms after the emission of a spontaneous photon, as will be detailed below.

The overall excitation probability p_e can be written as

$$p_e = p_{\mathrm{HF}} + p_{\mathrm{LF}} + p_{\mathrm{inc}}, \tag{2a}$$

$$p_{\mathrm{HF}} = 2\,\mathrm{Re}\{(B_0^+C_0^+B_0^-A_0^-)(D_0^+D_0^+D_0^-B_0^-)^* \times e^{i[4\pi(\nu_L-\nu_{\mathrm{Ca}}-\delta)T+\Phi_{1234}]}\}e^{-\gamma_a(T+2T_p)}, \tag{2b}$$

$$p_{\mathrm{LF}} = 2\,\mathrm{Re}\{(B_0^+A_0^+A_2^-A_2^-)(D_0^+B_0^+C_2^-B_2^-)^* \times e^{i[4\pi(\nu_L-\nu_{\mathrm{Ca}}+\delta)T+\Phi_{1234}]}\}e^{-\gamma_a(T+2T_p+T')}. \tag{2c}$$

The instantaneous phases of the laser beams at the point of interaction are imprinted on the wave functions that leads to an overall phase shift of

$$\Phi_{1234} = \phi_2 - \phi_1 + \phi_4 - \phi_3 \tag{3}$$

for both interferometers.

The coefficients A to D in Eq. (2) describe the interaction of the atom with a single laser pulse and can in general be obtained by solving the optical Bloch equation [20] for the actual excitation pulses. Similar to the complex coefficients for the reflection and transmission of amplitudes in an optical beamsplitter, A and D describe the probability amplitude for an atom staying in the excited and ground state, respectively, while B and C are the amplitudes for the atom changing to the excited and ground state, respectively. In the case of rectangular pulses of duration T_p, the coefficients are

$$A_m^{\pm} = D_m^{\pm *} = \cos\left(\frac{\Omega_m^{\pm}T_p}{2}\right) + i\frac{\Delta_m^{\pm}}{\Omega_m^{\pm}}\sin\left(\frac{\Omega_m^{\pm}T_p}{2}\right), \tag{4a}$$

$$B_m^{\pm} = -C_m^{\pm *} = i\frac{\Omega_R}{\Omega_m^{\pm}}\sin\left(\frac{\Omega_m^{\pm}T_p}{2}\right). \tag{4b}$$

Here $m=0,2$ denotes the number of additional photon recoils that were transferred to the atom before the respective interaction with the laser beam of direction $\pm$ (see Fig. 4). The coefficients

$$\Delta_m^{\pm} = 2\pi\left(\nu_L - \nu_{\mathrm{Ca}} \mp \frac{v\nu_{\mathrm{Ca}}}{c_0} + (\mp 2m-1)\delta\right), \tag{5a}$$

$$\Omega_R = \sqrt{\frac{3c_0^2\gamma_a I}{2\pi h\nu_{\mathrm{Ca}}^3}}, \tag{5b}$$

$$\Omega_m^{\pm} = \sqrt{\Omega_R^2 + \Delta_m^{\pm 2}} \tag{5c}$$

are the effective detunings $\Delta_m^{\pm}$ between ν_{Ca} and the frequency of the interacting laser seen by the atom, the resonant Rabi frequency Ω_R and the effective Rabi frequencies $\Omega_m^{\pm}$ for the nonresonant interaction with the laser pulses.

The frequency dependence of the interference terms is mainly due to the argument in the exponential of Eq. (2). However, also the coefficients from Eq. (4) show a small dependence on the laser frequency. This can be taken into account by using an effective pulse separation $T_{\mathrm{eff}}=T+\eta T_p$ for calculation of the fringe period Δ_{fringe},

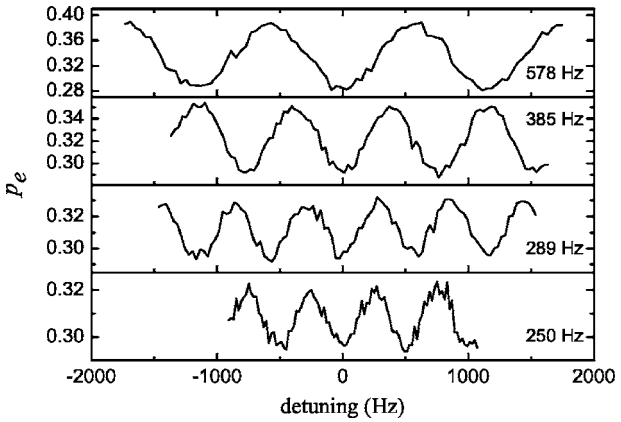

FIG. 5. Interference fringes in an asymmetric Ramsey-Bordé interferometer at different resolutions using ultracold atoms (12 μK) and a shelving detection scheme (see Sec. III D). No averaging was used.

$$\Delta_{\text{fringe}} \approx \frac{1}{2(T+\eta T_{\text{p}})}, \tag{6}$$

with $\eta=4/\pi$ for near resonant rectangular pulses [21]. The resolution is given as the half-width of the fringes, i.e.,

$$\Delta = \frac{\Delta_{\text{fringe}}}{2} = \frac{1}{4(T+\eta T_{\text{p}})}. \tag{7}$$

The two recoil patterns have the same period, but are shifted with respect to each other by twice the recoil shift δ, each one centered at $\nu_{\text{Ca}}\pm\delta$ for the high (HF) and low frequency (LF) component, respectively. Optimal contrast is achieved by setting the resolution to an integer fraction of the recoil splitting 2δ, i.e.,

$$T+\eta T_{\text{p}} = \frac{n}{2\delta}, \tag{8}$$

which allows for the two interference patterns to add constructively.

Figure 5 shows interference patterns close to ν_{Ca} for different resolutions. The decrease in excitation probability and contrast with increasing resolution is in part due to the decay of the excited clock state during atom interferometry. This is contained in Eq. (2) in the real exponential terms.

So far, the phases ϕ_i of the excitation pulses were regarded as constant, but deviations may occur due to imperfect wavefronts or rapid phase fluctuations. We describe the electric field E of the laser beams at position $\vec{r}(t_l)$ at the time t_l by an approximately plane wave with wave vector $\vec{k}_l$ as

$$E_l(\vec{r},t) = \text{Re}[E_{l0}(\vec{r})e^{i[2\pi\nu_{\text{L}}t-\vec{k}_l\vec{r}+\phi(\vec{r},t)]}], \tag{9}$$

where all deviations from a plane wave are contained in the time and spatial dependent phase $\phi(\vec{r},t_l)$.

This is especially important in combination with a residual Doppler effect [22,23] (see Sec. IV A). During the short interaction times of $T_{\text{p}}\approx 1$ μs, we neglect the movement of the atoms. With Eq. (9), we thus obtain

$$\phi_l = -\vec{k}_l\vec{r}(t_l) + \phi(\vec{r}(t_l),t_l). \tag{10}$$

In the calculation of Ref. [19], leading to p_{HF} and p_{LF} in Eq. (2), atoms do not contribute to the signal if a spontaneous emission has occurred during interferometry. While this correctly describes the decreases of the amplitude of the interference terms, these atoms can be reexcited in a later pulse and therefore still contribute to the incoherent background. The probability for a reexcitation of these atoms is dependent on the overlap of the single pulse excitation profile and the Doppler shift due to the recoil of the previously absorbed and emitted photons. Usually the Fourier width of the excitation pulse is much larger than the recoil shift, so this reexcitation probability is close to one. To describe this background realistically, the complete incoherent background p_{inc} was calculated from the incoherent evolution of the atomic population Π during the interferometric sequence. For interaction with a single laser pulse that couples the two momentum states $|g,p\rangle$ and $|e,p+\hbar k\rangle$ with the atom in the ground or excited state respectively, the corresponding populations $\Pi_{\text{g},p}$ and $\Pi_{\text{e},p+\hbar k}$ evolve according to

$$\begin{pmatrix}\Pi_{\text{e},p+\hbar k}\\ \Pi_{\text{g},p}\end{pmatrix}' = \begin{pmatrix}|A|^2 & |B|^2\\ |C|^2 & |D|^2\end{pmatrix}\begin{pmatrix}\Pi_{\text{e},p+\hbar k}\\ \Pi_{\text{g},p}\end{pmatrix}, \tag{11}$$

where the prime denotes the population after the interaction.

During the dark time $T_{\text{sep}}=T$ or T' between the pulses spontaneous emission lead to a decrease of the excited state population,

$$\Pi'_{\text{e},p\pm\hbar k} = e^{-\gamma T_{\text{sep}}}\Pi_{\text{e},p\pm\hbar k}. \tag{12}$$

The change in the ground state population is complicated by the fact, that on spontaneous emission an additional recoil is acquired by the atom. The recoil is distributed according to the dipole pattern of the $\Delta m=0$ transition. Along the direction z of the laser pulse, which is perpendicular to the quantization axis, the probability density $P(p_z)$ for the component $p_z\in[-\hbar k,\hbar k]$ of the recoil momentum is therefore given by

$$P(p_z) = \frac{3}{8\hbar k}\left(1+\frac{{p_z}^2}{\hbar^2k^2}\right). \tag{13}$$

Because of the additional recoils from absorption and spontaneous emission, the contribution due to reexcited atoms can lead to line shape asymmetries. Also the incoherent background for atoms that did not experience spontaneous emission is not centered at the atomic line center. For example, for atoms at rest it is shifted by one recoil shift δ towards higher frequencies. As asymmetries can influence the measured frequency, a numerical simulation of these effects was performed. To simplify the numerical calculation, discrete momentum classes with a width of one recoil momentum $\hbar k$, centered around the initial momentum p are used, which is justified as the Fourier width of the laser pulses and the Doppler width of the atomic velocity distribution is much larger than the recoil shift. The probability for the atom to decay back to the initial momentum class is then given by

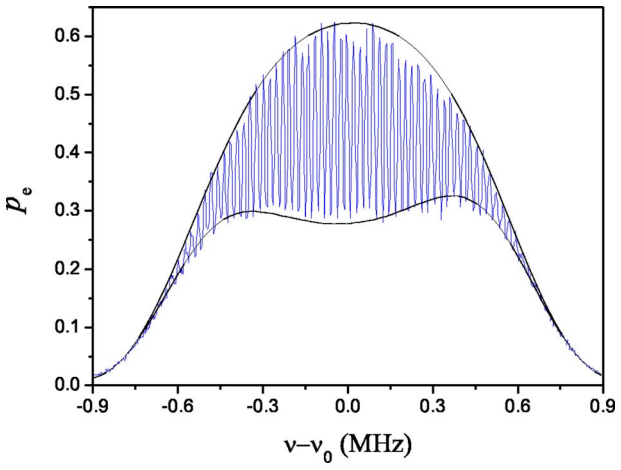

FIG. 6. (Color online) Interference signal using ultracold atoms (12 μK) and fluorescence detection. The lines denote the maximum and minimum as obtained from a Monte Carlo simulation.

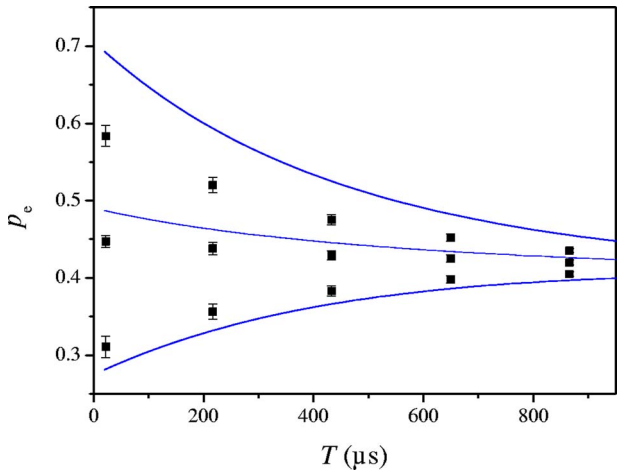

FIG. 7. (Color online) Measured excitation probability (squares) at maximum, center, and minimum of the interference signal as a function of the pulse separation time T and theoretical prediction (solid lines) for the experimental parameters.

$$P_0 = \int_{-\hbar k/2}^{\hbar k/2} P(p_z)dp_z = \frac{36}{96}, \tag{14}$$

and the probability to change the momentum class by $\pm\hbar k$ is $p_\pm = 30/96$. This calculation, assuming $\pi/2$ pulses, yields a background on resonance close to 0.5 independent of the pulse separation.

C. Comparison between theory and experiment

We have simulated the signal using the interference pattern from Eq. (2) and the background from Eq. (12). Using a Monte Carlo technique, the initial velocities and positions of several thousand atoms is randomly chosen from Gaussian distributions. The coefficients according to Eq. (4) are calculated at the positions of the individual atoms, taking into account the irradiance profile of the laser beams. Figure 6 shows a comparison between the experiment and the calculation for an ultracold ensemble of 12 μK with a pronounced asymmetry induced by the influence of the atomic recoil. This asymmetry strongly depends on the Doppler width and hence on the velocity of the atoms and on the Fourier width associated with the duration of the interrogating laser pulses [24]. The magnitude of possible frequency shifts due to the asymmetry of the spectrum have been obtained from this Monte Carlo simulation (see Sec. IV H) using the actual experimental conditions. The Monte Carlo simulations also can be compared with the experimentally observed minimum, maximum and average excitation probability (Fig. 7) and allow one to estimate the uncertainty of the associated corrections.

D. Shelving detection scheme

After performing the atom interferometric sequence, the excitation probability has to be measured. One possibility is to count the fluorescence photons from the decay of the $4s4p\ ^3P_1$ state. Due to the limited solid angle of the detection system and the efficiency of the photomultiplier tube, the detection probability per atom is on the order of 10^{-3}. Thus, the signal-to-noise ratio (SNR) is dominated by the shot noise of the counted photons.

As an alternative a shelving detection method was used which allows a much better SNR. Directly after performing the atom interferometry, a laser pulse of 60 μs duration resonant with the $^1S_0$-$^1P_1$ transition at 423 nm with parameter $s_0 \approx 1$ excites the atoms. The measured blue fluorescence signal I_1 of this first detection pulse is proportional to the number of atoms which are in the ground state after the interferometry. After the detection pulse the atoms have been accelerated to a velocity of approximately 20 m/s. Before applying the second detection pulse, a delay of 1 ms is inserted. During this time the accelerated atoms move about 20 mm and thus leave the detection region. The lifetime of the excited state of the clock transition is 430 μs (see the Appendix), so approximately 90% of the atoms are excited after the AI decay during the delay time. With the quench laser present, as in some of the measurements reported here, nearly 100% of the atoms decay to the ground state during that delay. Therefore, the fluorescence signal I_2 of the second detection pulse is proportional to the number of atoms in the excited state directly after the interferometry with the same proportionality factor as in the first pulse. Thus, the excitation probability can be obtained through $p_e = I_2/(I_1+I_2)$.

E. Stabilizing the laser to the clock transition

To generate the error signal for the stabilization of the laser to the clock transition of Ca that is insensitive to a linear and quadratic background of the signal, a digital version of the third harmonic detection method [25] is used. Close to the resonance the interferogram has a sinusoidal shape. The excitation probability at four detunings $\nu_L - \frac{3}{2}\Delta$, $\nu_L - \frac{1}{2}\Delta$, $\nu_L + \frac{1}{2}\Delta$, $\nu_L + \frac{3}{2}\Delta$ on the steepest slopes of the interferogram are measured for the generation of the error signal.

If we characterize the shape of the interference signal using the contrast $C = (p_{max} - p_{min})/(p_{max} + p_{min})$ and the mean

excitation probability p_m for small detunings $\Delta\nu_L$ of the laser frequency from the clock transition frequency the deviation is given by

$$\Delta\nu_L = -\frac{\Delta}{2\pi p_m C}\frac{1}{8}\left[p_e\left(\nu_L - \frac{3}{2}\Delta\right) - 3p_e\left(\nu_L - \frac{1}{2}\Delta\right) + 3p_e\left(\nu_L + \frac{1}{2}\Delta\right) - p_e\left(\nu_L + \frac{3}{2}\Delta\right)\right]. \quad (15)$$

After measuring the excitation probability p_e at all four detunings during eight trapping cycles of length T_c each, $\Delta\nu_L$ is calculated and the laser frequency is corrected by a fraction $\beta\Delta\nu_L$ of the full deviation. In successive stabilization cycles the direction of the frequency steps is reversed to cancel out errors due to a linear laser frequency drift and the duration of the measurement. This scheme corresponds to a single integrator with a time constant τ_β for the stabilization given by $\tau_\beta = -T_s/\ln(1+\beta)$ where $T_s = 8T_c$ denotes the time for one whole stabilization cycle. For the measurements the values were set to $\beta = -0.4$ resulting in $\tau_\beta \approx 5$ s.

If the laser frequency would be corrected only proportional to the measured deviation with a gain factor β, a frequency drift δ_t of the free running laser due to the reference cavity drift (Sec. III A) would result in a constant offset $\Delta\nu_L = -\delta_t T_s/\beta$. Therefore, the actual value of the drift is calculated as a running exponential average from the previous stabilization measurements with a time constant of $\tau_\alpha = 1000$ s, and the frequency ν_L in each cycle is corrected for this drift.

F. Method of alternating stabilization

To identify the influence of an arbitrary parameter, e.g., the density of the atomic ensemble, on the transition frequency of the intercombination line, an alternating stabilization scheme is used [26,27]. It consists of two stabilization schemes that are interlaced in time. From one trapping and interrogation cycle to the next, the experimental conditions are switched and the corresponding stabilization is performed for each parameter set independently (with a common correction of the drift). With this scheme it is possible to determine the frequency difference between two parameter settings without measuring the absolute frequency change, by relying on the reference resonator as a flywheel for times in the order of the cycle time. At the same time systematic shifts, like the first order Doppler effect, that are common to both conditions are largely suppressed. Both stabilizations are offset in time by the duration of one trapping and cooling cycle ($T_c \approx 0.5$ s). Because the drift of the laser is monitored during the stabilization, it could be easily corrected for. However, as the drift was below 0.05 Hz/s, at present the correction of 25 mHz was neglected.

IV. SYSTEMATIC UNCERTAINTIES

The aspects discussed in this section were partly already addressed in previous papers [3,28]. The discussion now also includes the underlying experimental conditions from which the uncertainty contributions and frequency corrections are derived.

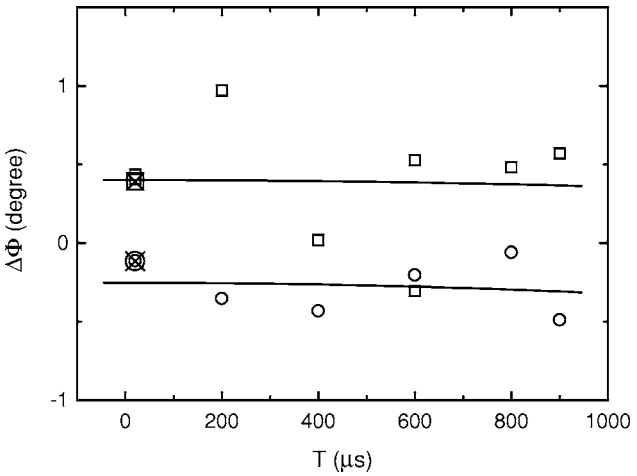

FIG. 8. Phase shift in a symmetric three pulse interferometer for different pulse separations. Squares and circles denote the two directions of spectroscopy. The solid lines are parabolas fitted to the data. The crossed square and the crossed circle denote the calculated shifts due to temporal phase excursions in the spectroscopy beams (Sec. IV B).

A. Residual Doppler effect

The term "residual Doppler effect" summarizes contributions which stem from the residual motion of the atoms during the atom interferometry and their acceleration due to gravity. Since the phase of the exciting laser beams is imprinted onto the phase of the atomic wavepackets, curved wavefronts and tilted beams with respect to gravity lead to parasitic frequency shifts. Assuming spherical wavefronts, phase and frequency shifts in symmetric and asymmetric atom interferometers can be related to each other [23].

It is therefore possible to calculate the frequency shift in the asymmetric four pulse interferometers by the determination of phase shifts in the symmetric three pulse interferometers. Figure 8 shows the phase shifts measured in a symmetric three pulse interferometer. To minimize the phase shifts, the wavefronts were optimized by means of an optical shearing interferometer. After that the tilt of the spectroscopy beams was adjusted in such a way that the phase shift at the largest pulse separation used ($T = 900$ μs) corresponds to the shift at the smallest separation ($T = 20$ μs). The constant residual shift independent of T of approximately half a degree is caused by phase excursions during the excitation pulses (Sec. IV B). Parabolas were fitted to the data of Fig. 8 yielding $A_\uparrow = (-0.4 \pm 5.1) \times 10^5$ degree/s^2 and $A_\downarrow = (-0.7 \pm 2.6) \times 10^5$ degree/s^2, where $\uparrow$ and $\downarrow$ represent the two opposite directions of the interrogating pulses. According to [23], this leads to a frequency shift of

$$\Delta\nu_{\uparrow\uparrow\downarrow\downarrow,T} = (-0.1 \pm 0.9)\ \text{Hz} - (1.7 \pm 9.0) \times 10^{-4}\frac{\text{Hz}}{\mu\text{s}}T. \quad (16)$$

The main contribution of (-0.1 ± 0.9) Hz results from the delay time $T_1 = 800$ μs between turning off the MOT and the

first spectroscopy pulse. With a better synchronization of the mechanical shutters and choppers used, this time could be reduced to 200 μs, corresponding to an uncertainty contribution of below 0.3 Hz.

The resolution-dependent part in Eq. (16) amounts to (-0.08 ± 0.42) Hz and (-0.04 ± 0.21) Hz, respectively, for the pulse separations used in the frequency measurement ($T+T_p=454.5$ μs and 216.4 μs).

In addition to this resolution-dependent term, a constant frequency shift exists for which an upper limit can be estimated [23] to

$$\Delta\nu_{\uparrow\uparrow\downarrow\downarrow,0,\max} = \sqrt{\left(\frac{k|\vec{v}_0|}{4\pi}\Theta\right)^2 + \left(\frac{k|\vec{v}_0||\vec{r}_0|}{4\pi}\frac{2}{\min(R_\uparrow,R_\downarrow)}\right)^2} = 0.53 \text{ Hz}.$$

The center of mass velocity was determined as $|\vec{v}_0|=1.6$ cm/s. The offset $|\vec{r}_0|$ was smaller than 0.5 mm. $R_\uparrow$ and $R_\downarrow$ are the radii of curvature of the two spectroscopy beams, which were bigger than 40 m. The angle Θ between the two beams was smaller than 2×10^{-3} degree. k is the wave number of the spectroscopy beams. For a rectangular distribution between $-\Delta\nu_{\uparrow\uparrow\downarrow\downarrow,0,\max}$ and $\Delta\nu_{\uparrow\uparrow\downarrow\downarrow,0,\max}$ the corresponding standard uncertainty [29] reads

$$u(\Delta\nu_{\uparrow\uparrow\downarrow\downarrow,0}) = \frac{\Delta\nu_{\uparrow\uparrow\downarrow\downarrow,0,\max}}{\sqrt{3}} = 0.31 \text{ Hz}. \quad (17)$$

Together with the resolution-dependent frequency shift [Eq. (16)], the total contribution of the residual Doppler effect to the uncertainty budget is estimated to be 1.0 Hz.

B. Phase excursions in the excitation pulses

Besides phase shifts that appear due to the motion of the atoms, also phase shifts of the light pulses itself might lead to unwanted frequency shifts. Initially, mechanical movements of mirrors in the path of the spectroscopy pulses were induced by acoustic transients from the mechanical switches used to block the trapping beams. This movements of a few nanometers lead to quite constant phase shifts of several milliradian in the spectroscopic signal. To avoid these problems, the shutters were completely isolated from the optical table.

Another source of parasitic phase shifts lies in the AOM that cut the excitation pulses from the cw laser beam, e.g., because of a heating or because of electronic phase shifts. This effect has been treated in detail elsewhere [30] and it suffices here to give the results. The optical phase of the excitation pulses was determined with a homodyne interferometer. For pulse length of up to 30 ms, a linear variation of the phase of $(\Delta\varphi)/(\Delta t)=2\times10^{-7}$ degree/μs is observed. This corresponds to a frequency shift of less than a millihertz which can be neglected.

Large phase excursions at the edges of the pulses were observed. The form of the excursions depend sensitively on the alignment and driving frequency of the AOM and the input coupling into the fibers. Changing the length of the coaxial cable between the amplifier and the AOM also changes the phase excursions. In contrast, changing the rf power by a factor of four does not change the phase excursions significantly. Also the length of the pulse shows no influence on the excursions in the edges of the pulse. We therefore attribute the ringing of the phase to the bandpass character of the total transfer function from rf to the optical signal behind the optical fiber.

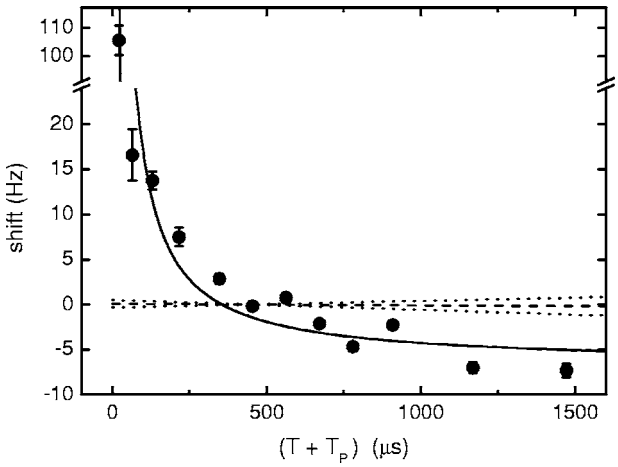

FIG. 9. Influence of the phase excursions on the resolution-dependent frequency shift in a four pulse interferometer. The graph shows the frequency shift for a pulse separation $T+T_p$ relative to the shift for a separation of 454.5 μs at an rf frequency of 81 MHz. The solid line is a fit to the data (see text). The dashed line indicates the shift due to curved and tilted wave fronts of the spectroscopy pulses with its uncertainty interval (dotted lines).

To correct the influence of the phase excursions, the frequency shift in an asymmetric four pulse interferometer was measured for pulse separations T between 20 μs and 1472 μs and an rf frequency of 81 MHz (Fig. 9), using a separation of 454 μs as reference. The dashed line shows the shift expected for curved and tilted spectroscopy beams as determined by using three pulse interferometers with their uncertainty (dotted lines). The function $\Delta\nu=A+B/(T+T_p)$ was fitted to the data taking into account the uncertainty of the dashed line. For the pulse separations and the rf frequency (81 MHz) used during the frequency measurement ($T+T_p=216.4$ μs and 454.5 μs), the corrections that must be applied are (-11.1 ± 1.7) Hz and (-5.3 ± 1.6) Hz.

C. Collisional shifts

Interactions between the atoms of the ultracold ensemble, i.e., cold collisions, lead to frequency shifts of the clock transition. In present Cs fountain clocks this effect constitutes one of the main contributions to the uncertainty. Our first investigation of collisions in the calcium frequency standard [23] made use of cold ensembles at 3 mK. Calculations for the collisional shift in caesium have shown a possible dramatic variation of the shift with temperature. Therefore, it was necessary to examine the influence of collisions with ultracold ensembles. A detailed more description of these measurements is given in Refs. [3,28].

One finds for the collisional frequency shift A_ρ relative to the frequency of the clock transition ν_{Ca} at $T=20$ μK

$$\frac{A_\rho}{\nu_{\mathrm{Ca}}} = (-0.4 \pm 1.2) \times 10^{-31}\ \mathrm{m}^3. \tag{18}$$

Since the statistical uncertainty of A_ρ seems too small concerning the scatter in the measured data, the uncertainty was determined by an alternative way. Over the whole range of density differences $\Delta\bar{\rho}$, the standard deviation of the measured frequency shifts amount to 0.7 Hz. This value was assumed as the uncertainty at the highest density differences realized in the experiment of $\Delta\bar{\rho}=1.2\times10^{16}\ \mathrm{m}^{-3}$.

For mean densities of $1\times10^{15}\ \mathrm{m}^{-3}$, as used in the frequency measurement, a collisional shift of (-20 ± 55) mHz results, corresponding to a relative shift of $(-0.4\pm1.2)\times10^{-16}$. Compared to the relative collisional frequency shift in ^{133}Cs [31,32] the density dependence is four orders of magnitude smaller and also smaller than the shift of the intercombination line of Sr [33].

D. Magnetic fields

The $^3P_1(m=0)$ level exhibits a small second order Zeeman shift that was calculated to be $(6.375\pm0.009)\times10^7\ \mathrm{Hz/T^2}$ [34]. The diamagnetic shift of the $^1S_0(m=0)$ level amounts to less than 1% of this value. The quadratic Zeeman-effect of the line was measured in calcium atomic beams and laser cooled ensembles [34–36] resulting in $(6.4\pm0.1)\times10^7\ \mathrm{Hz/T^2}$. This value is used to correct the frequency shift due to a homogeneous bias magnetic field that separates the $m=\pm1$ Zeeman components from the $m=0$ component. The magnitude of the bias field was measured to be 0.18 mT by determining the splitting of the $m=\pm1$ Zeeman components that shift with $\pm2.1\times10^{10}$ Hz/T. Nevertheless, 50 Hz oscillations in the current of the power supply used to generate the bias field lead to oscillations in the magnetic field of 2 μT.

All other magnetic fields like the Earth's magnetic field have to be compensated for. For this purpose compensation fields in three dimensions are used. The magnitude of the remaining magnetic field after compensation was measured using the crossover effect of the Zeeman-lines in saturation spectroscopy. For times $T_1 \geqslant 200\ \mu$s after switching off the magnetic quadrupole field of the trap, the value was less than 4 μT. The uncertainty in the magnitude of the magnetic field is assumed to be 4 μT resulting in a quadratic Zeeman shift of $\Delta\nu_{\mathrm{QZ}}=(2.12\pm0.1)$ Hz.

E. dc Stark effect

External electric fields can shift the transition frequency due to the Stark effect. The main contributions to an electric dc field in our setup originate from static loads of the surface of the stainless steel vacuum chamber or the kapton-coated magnetic field coils. We assume a maximum field of 200 V/m at the position of the trap. The atomic states participating in the Stark effect on the clock transition are all of defined parity. Therefore, there are no contributions to the Stark effect with an odd dependence on the electric field. Zeiske [37] showed that with these electric fields higher order contributions only lead to shifts in the microhertz range. Hence, only the quadratic Stark effect needs to be taken into account and the frequency shift $\Delta\nu_{\mathrm{QS}}$ of the clock transition is given by

$$\Delta\nu_{\mathrm{QS}} = -\frac{1}{2h}\Delta\alpha E^2. \tag{19}$$

The difference of the polarizabilities $\Delta\alpha$ of the two clock states was determined [37] to $\Delta\alpha_\sigma/h=(3.37\pm0.04)\times10^{-6}\ \mathrm{Hz/(V/m)^2}$ for an electric field perpendicular to the quantization axis of the atoms and $\Delta\alpha_\pi/h=(2.47\pm0.04)\times10^{-6}\ \mathrm{Hz/(V/m)^2}$ for a field parallel to the quantization axis. As the polarization of a static electric field is likely to remain constant but is not known, an arbitrary distribution of the polarity as well as the absolute value of the electric field $\vec{E}$ between 0 and 200 V/m is assumed. Averaging over possible polarities and field strengths yields a correction of (35 ± 22) mHz.

F. ac Stark effect

The laser radiation used for cooling and spectroscopy can cause ac Stark shifts of the clock transition if it is incident on the region of the atoms during probing the clock transition. In second order perturbation theory, the energy shift $U_i(\omega,p,m_i)$ of an atomic state i with energy E_i and Zeeman level m_i, which is induced by a perturbing laser field with frequency $\nu=\omega/2\pi$, polarization p, and irradiance I, can be expressed as $U_i(\omega,p,m_i)=-\alpha_i(\omega,p,m_i)I/2\epsilon_0 c$. The induced polarizability α_i was calculated by summing the contributions from all dipole transitions from the desired state i to levels k with the respective Einstein coefficients A_{ki} (spontaneous emission rate for $E_k>E_i$), Zeeman levels m', and transition frequencies $\nu_{ik}=\omega_{ik}/2\pi$ [38]

$$\alpha_i = 6\pi c^3 \epsilon_0 \sum_{k,m'} \frac{A_{ki}(2J_k+1)}{\omega_{ik}^2(\omega_{ik}^2-\omega^2)} \begin{pmatrix} J_i & 1 & J_k \\ m_i & p & -m' \end{pmatrix}^2. \tag{20}$$

The $3J$ symbol, see, e.g., [39], describes the selection rules and relative strengths of the transitions depending on the involved angular momenta J, their projections m and the polarization p.

The transition frequencies and A_{ki} coefficients were taken from the comprehensive data collection of Kurucz [40]. Additionally, the influence of the continuum and highly excited states was approximated by using hydrogen wavefunctions [41] similar to the method of von Oppen [42].

First, there are contributions from very far detuned laser sources, e.g., pump lasers. With a total irradiance of $\approx1\ \mathrm{W/m^2}$, the resulting frequency shifts are well below one mHz. Secondly, since the near resonant trap and quench laser beams are switched by acousto-optical modulators, even in the switched off state scattered light can reach the atomic ensemble, leading to frequency shifts of a few ten Hertz. Therefore, all trapping laser beams and the quench laser beam were additionally blocked by mechanical shutters during the time of atom interferometry. The laser beam for shelving detection was blocked by a mechanical chopper to allow for fast switching times. As a third contribution,

3 mW/m^2 stray light in the spectroscopy beams detuned by 81 MHz from the clock transition leads to a shift of a few mHz only.

In total, the residual frequency shift of a few mHz due to the ac Stark effect can be neglected.

G. Blackbody radiation

The energy shift ΔE_i of an atomic level i by the ac Stark shift due to blackbody radiation of temperature T_{env} can be calculated according to [43]

$$\Delta E_i(T_{\mathrm{env}}) = -\frac{\hbar}{2\pi}\left(\frac{k_B T_{\mathrm{e}}}{\hbar}\right)^3 \sum_k \frac{2J_k+1}{2J_i+1}\frac{A_{ki}}{\omega_{ik}^3} F\left(\frac{\hbar\omega_{ik}}{k_B T_{\mathrm{env}}}\right), \tag{21}$$

where

$$F(y) = \int_0^\infty \frac{x^3}{e^x-1}\left(\frac{1}{y-x}+\frac{1}{y+x}\right)dx \tag{22}$$

contains the integration across the blackbody spectrum.

As all transitions have energies much larger than the thermal energy, this can be written as a quasistatic shift that depends on the scalar polarizability α_{scal} plus a small correction

$$\Delta E_i(T_{\mathrm{env}}) = -\frac{\alpha_{\mathrm{scal}}}{2}\langle E^2\rangle - \frac{\hbar}{2\pi}\left(\frac{k_B T_{\mathrm{env}}}{\hbar}\right)^3 \sum_k \frac{2J_k+1}{2J_i+1}\frac{A_{ki}}{\omega_{ik}^3} G\left(\frac{\hbar\omega_{ik}}{k_B T_{\mathrm{env}}}\right), \tag{23}$$

with

$$G(y) = \int_0^\infty \frac{x^3}{e^x-1}\left(\frac{1}{y-x}+\frac{1}{y+x}-\frac{2}{y}\right)dx \approx \frac{16\pi^6}{63y^3} \tag{24}$$

and the mean square of the electric field $\langle E^2\rangle$ at temperature T_{env}

$$\langle E^2\rangle = \frac{8\pi^5 k_B^4}{15 c_0^3 \epsilon_0 h^3} T_{\mathrm{env}} = 8.545\times 10^{-5}\ \frac{\mathrm{V}^2}{\mathrm{m}^2\mathrm{K}^4} T_{\mathrm{env}}^4. \tag{25}$$

In contrast to the treatment given in Ref. [28], this description goes beyond the static approximation. As the difference of the static polarizabilities was measured precisely by Li and van Wijngaarden [44] to $\Delta\alpha_{\mathrm{scal}}/h = (29.874\pm 0.087)\ \mathrm{kHz}/(\mathrm{kV/cm})^2$, the frequency shift due to the room temperature environment of the water cooled copper coils and the vacuum chamber with a temperature $T_{\mathrm{env}} = (293\pm 5)$ K is calculated to be (-970 ± 70) mHz including a correction of -40 mHz due to the deviation from the quasistatic approximation. So even as the Einstein A_{ki} coefficients are not precisely known, their uncertainty does not significantly contribute to the uncertainty of the blackbody shift.

Since the oven that produces the effusive beam of calcium atoms (Sec. II) is only 15 cm away from the trapped ensemble its blackbody radiation can exert a strong ac Stark shift. A temperature bath of $T_{\mathrm{e}} = 900$ K would result in a shift of -120 Hz. The actual influence of the oven is strongly reduced due to its small surface that is mostly hidden by the geometry of the vacuum chamber. However, it is hardly possible to calculate the exact influence of the oven, since this would require a detailed treatment of all reflections of the blackbody radiation inside the vacuum chamber. Therefore, the frequency shift was determined during the frequency measurements of 2001 and 2003 by changing the oven temperature from 900 K to 800 K. From this the shift can be estimated to be (-2.8 ± 3.9) Hz. At present, this is the largest contribution to the uncertainty. In future experiments, the influence of the oven will be eliminated by using a Zeeman slower in combination with a deflection molasses.

H. Symmetry of the interference signal

The interference signal of the atom interferometry consists of the superposition of two patterns shifted by the recoil separation (Sec. III B). While it is possible to remove one of the recoil components [45,46], for the realization of the frequency standard that is reported here, the laser was stabilized to the central extremum of the sum of both recoil components. As long as the amplitudes of both recoil components are equal or if the period is exactly an integer fraction of the recoil splitting 2δ, this central extremum corresponds exactly to the atomic transition frequency ν_{Ca}.

However, there are asymmetries between both recoil components due to the different excitation probabilities and due to the spontaneous decay of excited atoms, that contribute to the low frequency component during central dark time $T' \approx 8\ \mu$s between the second and third pulse (see Fig. 4). Also the contribution of the pulse length to the effective pulse separation time depends on the laser irradiance at the position of the respective interaction [compare Eq. (4)]. Because of the expansion and the movement of the atomic cloud under the influence of gravity in a Gaussian irradiance distribution of the exciting pulses, this effect is difficult to estimate. We have therefore used Eqs. (2) and (4) with atomic trajectories chosen from a Gaussian distribution in position and velocity, to calculate the atomic signal in a Monte Carlo simulation. This simulation includes all discussed effects that lead to an asymmetry of the signal. It is therefore possible to determine quantitatively the associated frequency shifts.

To study the effectiveness of the $3f$ scheme in comparison with the $1f$ method, both locking methods were simulated with the Monte Carlo approach. The results for the resulting frequency offset from the true atomic line versus the pulse separation T are shown in Fig. 10, for the experimental parameters: 1D velocity (spatial) width 7.7 cm/s (0.35 mm), rectangular pulses of length $T_p = 1.5\ \mu$s and Gaussian beams of waist $w = 1.79$ mm. The power was adjusted to give the maximum excitation probability in a single pulse for a pulse length of 2 T_p in the same way as it is done in the experiment.

The pattern generator that controlled the timing of the pulses had a resolution of 100 ns. So the pulse separation

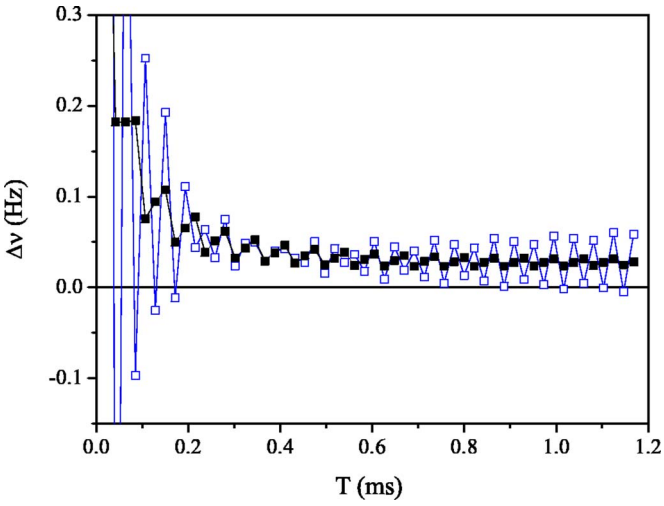

FIG. 10. (Color online) Simulation of the $1f$ (open squares) and $3f$ stabilized (filled squares) frequency offsets from the unperturbed calcium frequency at different resolutions using 100 000 ultracold atoms at 12 μK and $x_{\mathrm{rms}}=0.35$ mm. The pulse width was $T_{\mathrm{p}}=1.5$ μs and the central dark time $T'=1.5$ μs.

time had to be rounded to the nearest multiple of 100 ns, which introduced additional errors. They show up as fluctuations of the $3f$ values in Fig. 10. The resulting frequency shift was smaller than 0.2 Hz at the resolution settings of the frequency measurement.

V. FREQUENCY MEASUREMENT

The transition frequency of the calcium intercombination line at 657 nm was determined with respect to the primary standard of time and frequency, the caesium clock, using a self-referenced optical frequency comb generator. The measurement took place on October 2003 for different parameter settings of the calcium standard. The pulse separation for the asymmetric four pulse interferometers was varied between 216.4 μs and 454.5 μs to examine frequency fluctuations due to phase excursions in the exciting laser pulses. The temperature of the calcium oven was varied between 900 K and 800 K to determine the influence of the blackbody shift. The blue and red MOT beams, the detection beam and the quench laser beam were blocked by mechanical shutters and choppers during the atom interferometry to prevent shifts due to the dynamic Stark effect.

Table I summarizes all contributions to the uncertainty budget of the calcium frequency standard. From the frequency measurements with different parameters, the weighted average was calculated. To derive the uncertainty of the weighted average the statistical and systematic uncertainty of the frequency measurement and the maximum uncertainty of the corrections were taken into account. Since the measurements are assumed to be correlated only the statistical uncertainty of the frequency measurement is reduced by the averaging. This results in a frequency of the $^1S_0(m=0)$ to $^3P_1(m=0)$ transition in ^{40}Ca of $\nu_{\mathrm{Ca}}=(455\,986\,240\,494\,144\pm5.3)$ Hz.

TABLE I. Uncertainty budget for the frequency measurement in October 2003.

Contribution	Shift $\Delta\nu=\nu-\nu_{\mathrm{Ca}}$	Uncertainty $u(\Delta\nu)$
Blackbody radiation		
oven (873 K)	−2.8 Hz	3.9 Hz
room temperature	−0.97 Hz	0.07 Hz
Laser phase		
temporal phase ($T+T_{\mathrm{p}}=454$ μs)	+5.3 Hz	1.6 Hz
spatial phase	−0.2 Hz	1.0 Hz
Line form asymmetry	0 Hz	0.2 Hz
Quadratic Zeeman effect	+2.12 Hz	0.1 Hz
Drift of resonator	0 Hz	0.1 Hz
Collisions	−0.02 Hz	0.06 Hz
Quadratic Stark effect	−0.04 Hz	0.02 Hz
Total	+3.4 Hz	4.3 Hz
$u(\Delta\nu)/\nu_{\mathrm{Ca}}$		1×10^{-14}
Frequency measurement	0 Hz	3.1 Hz
Sum in quadrature		5.3 Hz

Figure 11 summarizes all measurements of the clock transition in calcium since 1995. Until September 2000, a harmonic frequency multiplication chain was used [47]. Since June 2001 a femtosecond comb generator was used [48]. Between the measurement in October 2001 and the measurement presented here, besides using ultracold atoms for the first time, nearly the whole setup was changed, including the spectroscopy laser system, the frequency comb and the data acquisition system. Thus, the good agreement between the measurement in October 2001 and the last measurement shows that the current uncertainty of 10^{-14} is a realistic estimation. This is supported by frequency measurements of the

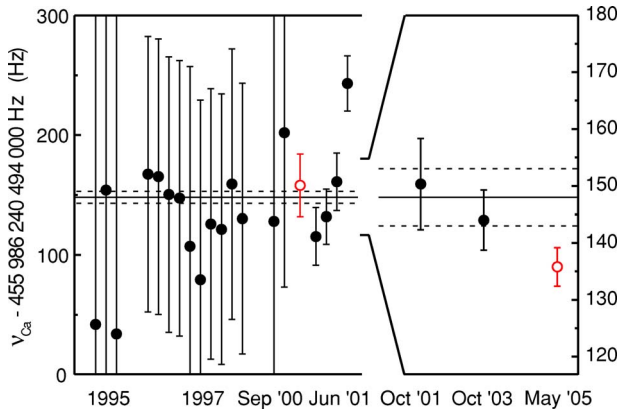

FIG. 11. (Color online) Summary of all frequency measurements performed at PTB (closed circles). Open symbols depict frequency measurements performed at NIST, Boulder. Until September 2000 a frequency chain was used. From June 2001 on a frequency comb generator was used. The line depicts the weighted mean of all PTB values with its uncertainty (dashed lines).

same transition in Ca at NIST, Boulder [49] that agree very well with the results from PTB.

VI. FREQUENCY STABILITY

Any noise in the interrogation of the atomic line is converted to frequency fluctuations once this signal is used to stabilize the laser frequency to the atomic transition. If the noise is white, i.e., uncorrelated between individual interrogations, then also the frequency noise of the locked laser averaged over times larger than the attack time of the locking servo is white. The corresponding frequency stability of the atomic frequency standard, described by the two-sample Allan standard deviation $\sigma_y(\tau)$ [50] then averages down like the inverse of the square root of the averaging time τ, as given by [50–52]

$$\sigma_y(\tau) = \frac{1}{\kappa}\frac{1}{Q}\sqrt{\frac{T_c}{\tau}}\left(\frac{\mathcal{N}}{\mathcal{S}}\right), \tag{26}$$

where $Q=\nu_{\mathrm{Ca}}/\Delta$ is the quality factor of the atomic line, and κ is a constant depending on the shape of the resonance. For a Ramsey-Bordé interferometer operated at the side of the central fringe, where the slope $\partial p_{\mathrm{e}}/\partial \nu_L$ is maximum, this constant is equal to $\kappa=\pi$ [21]. $\mathcal{S}$ denotes the signal amplitude and $\mathcal{N}$ the noise for a detection performed in a measurement cycle of duration T_{c}.

For the optical Ramsey fringe pattern, the result of the interrogation is the excitation probability p_{e} that can be approximated for small detunings including both recoil components as

$$p_{\mathrm{e}}(\nu_L) = p_{\mathrm{m}}\{1 + C\cos[4\pi(\nu_L - \nu_{\mathrm{Ca}})T]\}, \tag{27}$$

where C is the contrast of the Ramsey-Bordé fringes, and p_{m} the mean excitation probability. In Eq. (26) the signal amplitude $\mathcal{S}$ then corresponds to the fringe amplitude $\mathcal{S}=p_m C$ and the noise $\mathcal{N}$ to the standard deviation σ_{P_k} of a dataset of individual measurements of the excitation probability $\{P_k\}$ taken in regularly spaced intervals of duration T_{c}.

In the following we discuss the frequency stability by analyzing the independent noise contributions $\mathcal{N}_i$ as quantum projection noise, electronic noise, lasers noise, etc., that add quadratically:

$$\mathcal{S}/\mathcal{N} = \mathcal{S}\Big/\left(\sum_i \mathcal{N}_i^2\right)^{1/2}. \tag{28}$$

A. Noise sources

Noise contributions in the measurement of the transition probability experiment are listed and evaluated below. This analysis is performed for the experimental parameters during the frequency measurement: resolution $\Delta=550$ Hz, cycle time $T_{\mathrm{c}}=320$ ms, contrast $C=0.1$ and mean excitation probability $\langle P_k\rangle=p_{\mathrm{m}}=0.3$, leading to a signal amplitude of $\mathcal{S}=0.03$. These data are in agreement with simulations taking into account the spontaneous decay from the $^3P_1$ state, the temperature and the size of the atomic cloud. In that case, the line Q is $Q=8.2\times10^{11}$, leading to a factor in front of the parenthesis in Eq. (26) of 2.2×10^{-13} at $\tau=1$ s averaging time.

1. Quantum projection noise

The quantum projection noise (QPN) [53] contribution at an excitation probability p_{e} from N independent absorbers is given by

$$\mathcal{N}_{\mathrm{QPN}} = \sqrt{\frac{p_{\mathrm{e}}(1-p_{\mathrm{e}})}{N}}. \tag{29}$$

Due to the large number $N=3\times10^7$ of trapped ultracold atoms in our setup, one finds $\mathcal{N}_{\mathrm{QPN}}=8.3\times10^{-5}$ and $(\mathcal{S}/\mathcal{N}_{\mathrm{QPN}})^{-1}=2.8\times10^{-3}$. Thus, the quantum projection noise sets a quantum limit to the relative frequency stability of $\sigma_{y,\mathrm{QPN}}(1\ \mathrm{s})=6\times10^{-16}$ at 1 s averaging time.

2. Photon shot noise

Using the shelving detection method described in Sec. III D, each atom scatters many photons from which several are detected per atom. The photon shot noise (PSN) contribution appears in each of the two detection pulses and it leads to a noise in the measured excitation probability:

$$\mathcal{N}_{\mathrm{PSN}} = \sqrt{\frac{p_{\mathrm{e}}(1-p_{\mathrm{e}})}{n_{\mathrm{ph}}N}}, \tag{30}$$

where n_{ph} is the mean number of detected photons per atom in the ground state. As soon as more than one photon is detected per atom ($n_{\mathrm{ph}}>1$) this contribution becomes smaller than the QPN.

From direct measurements of the photocurrent and knowing the number of atoms in the MOT from density and size measurements, we determined the mean number of detected photons per atoms $n_{\mathrm{ph}}\simeq10$, corresponding to a total detection efficiency of about 1% of all scattered photons. One finds $\mathcal{N}_{\mathrm{PSN}}=2.6\times10^{-5}$, leading to a contribution to the relative frequency stability of $\sigma_{y,\mathrm{PSN}}(1\ \mathrm{s})=2\times10^{-16}$ at 1 s averaging time.

3. Electronic noise

Electronic noise is due to detector dark noise, amplifiers noises and A/D conversion noises (aliasing and sampling effects). We recorded the acquired noise with no atoms and no laser light, with the same acquisition time and sampling rate as during the real experiment. At the operating parameters of the clock, this noise amounts to $\mathcal{N}_{\mathrm{eln}}=9\times10^{-5}$, corresponding to a contribution to the relative frequency stability of $\sigma_{y,\mathrm{eln}}(1\ \mathrm{s})=7\times10^{-16}$ at 1 s averaging time. Even though the detector is an avalanche photo diode, during this work it was operated with a small bias voltage. Therefore no internal gain from the avalanche effect and therefore no additional noise appeared.

4. Detection-laser noise

An important noise source is related to the noise of the detection laser. Frequency fluctuations and power fluctuations of the detection laser lead to fluctuations of the spon-

taneous emission rate, and thus of the detected number of atoms. As the present shelving detection method uses a running wave, atoms are accelerated by the detection laser, leading to a change in the detuning during the 60 μs long detection pulses. By solving the equation of motion using the scattering force for a two-level atom, we find that atoms, that are initially in resonance with the blue laser pulse, are accelerated to a corresponding Doppler shift on the order of $\delta_D=40$ MHz at the end of the pulse, comparable to the natural line width Γ of the $^1S_0$-$^1P_1$ transition. The total number of scattered photons was calculated by integration of the time-dependent excitation rate during the pulse. Under the assumption of an rms frequency fluctuation of 200 kHz within the few milliseconds between the two adjacent detection pulses, we calculated a corresponding noise in the measured excitation probability of $\mathcal{N}_{\mathrm{fdet}}=1.4\cdot10^{-3}$ for the saturation parameter at resonance $s_0=1$ of the experiment.

The amplitude noise of the probe pulses was measured by detecting stray light of similar amplitude as the fluorescence with the same time sequence as in the usual experiment. We found fluctuations of the ratio κ between the signal from the first and the second pulse of $\sigma_\kappa=3\times10^{-2}$. By performing the calculation with these variations in the probe power, we found a noise contribution $\mathcal{N}_{\mathrm{adet}}=2.4\times10^{-4}$ at $s_0=1$. The quadratic sum of frequency and amplitude noise is $\mathcal{N}_{\mathrm{laser}}=1.4\times10^{-3}$. The contribution of the detection laser to the relative frequency stability is therefore as high as $\sigma_{y,\mathrm{laser}}(1\ \mathrm{s})=1.0\times10^{-14}$ at 1 s averaging time.

5. Dick effect

Even with the 1 Hz linewidth of the ultra-stable probe laser being much smaller than the atomic linewidth of 370 Hz, it significantly amounts to the frequency stability through the aliasing of the laser frequency noise in a discontinuous interrogation (Dick effect [54,55]). The Dick effect for an optical frequency standard with Ramsey-Bordé interrogation was first addressed by Quessada *et al.* [56]. This aliasing of spectral components of the probe laser's relative frequency noise $S_y(f)$ at harmonics of the cycle frequency $f_c=1/T_c$ of the clock leads to a frequency stability of the locked laser, given by

$$\sigma_y^2(\tau)=\frac{1}{\tau}\sum_{k=1}^{\infty}\left|\frac{g_k}{g_0}\right|^2 S_y\left(\frac{k}{T_c}\right), \tag{31}$$

where g_0 and g_k are the zeroth and kth Fourier component of the sensitivity function g [57], respectively. The sensitivity function g describes the change in the signal, i.e., the change in the excitation probability δp_e at the operational point of the frequency standard due to small frequency excursions of the probe laser $\delta\nu_L$ during one interrogation cycle from $t=0$ to T_c:

$$\delta p_e=\frac{1}{2}\int_0^{T_c} g(t)2\pi\delta\nu_L(t)dt. \tag{32}$$

For a 4-pulse asymmetric interferometer under optimum conditions of $\pi/2$ pulses and overlapping recoil components it is given as [56]

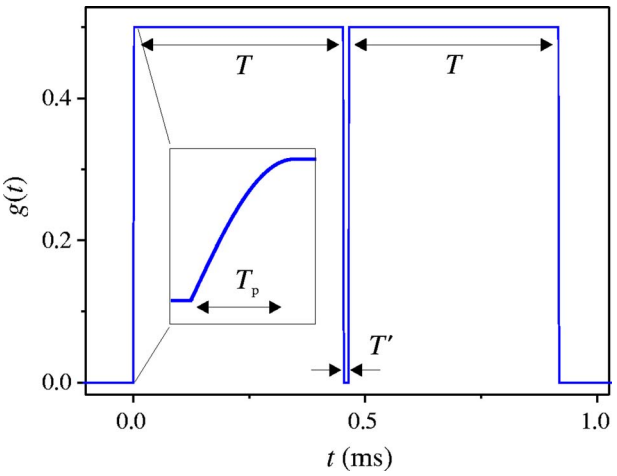

FIG. 12. (Color online) Sensitivity function for the 4-pulse Ramsey interrogation of the Ca-frequency standard. The inset shows the function during the first excitation pulse.

$$g(t)=\frac{1}{2}\times\begin{cases}\sin(\Omega t), & 0<t<T_p,\\ 1, & T_p<t<T_p+T,\\ \sin[\Omega(t-T)], & T_p+T<t<2T_p+T,\\ 0, & \text{otherwise}\end{cases} \tag{33}$$

for the first pair of pulses, and

$$g(t)=g[t-(2T_p+T+T')] \tag{34}$$

for the second pair of pulses (see Fig. 12).

As the durations of the excitation pulses are $T_p=(1-2)$ μs in the present experiment, which is $\sim10^5$ smaller than the cycle time T_c, the sine part in $g(t)$ modifies the g_k components only for harmonics above $f_2\approx200$ kHz where they change the slope to f^{-2}. Below that frequency the slope is approximately f^{-1} down to $f_1\approx1/2T$.

As the laser is stabilized to the atomic line using the $3f$ detection scheme of Sec. III E, there are 8 interrogation cycles, before the laser frequency is adjusted. Therefore, the full sensitivity function contains 8 copies of Eq. (33). This sensitivity function and the measured noise spectrum of the laser of interrogation (Fig. 13) was used with Eq. (31) to estimate the frequency stability due to the Dick effect to $\sigma_y(\tau)=2\times10^{-14}$ $(\tau/\mathrm{s})^{-1/2}$.

The quadratic sum of all the noise contributions is dominated by the Dick effect and the noise of the probe laser which leads to a relative frequency stability $\sigma_y=2.3\times10^{-14}$ at 1 s averaging time.

B. Measured signal-to-noise ratio

We have directly measured the noise $\mathcal{N}$ of the mean excitation probability on top, bottom, and half-middle of the central fringe. The noise of P_m at the top and bottom of the Ramsey fringes is to first order insensitive to frequency fluctuations of the interrogation laser. Therefore in this measurements, all noise sources except the Dick effect are measured. We found a noise $\mathcal{N}_{\mathrm{top}}=6\times10^{-3}$, and $\mathcal{N}_{\mathrm{bottom}}=2\times10^{-3}$,

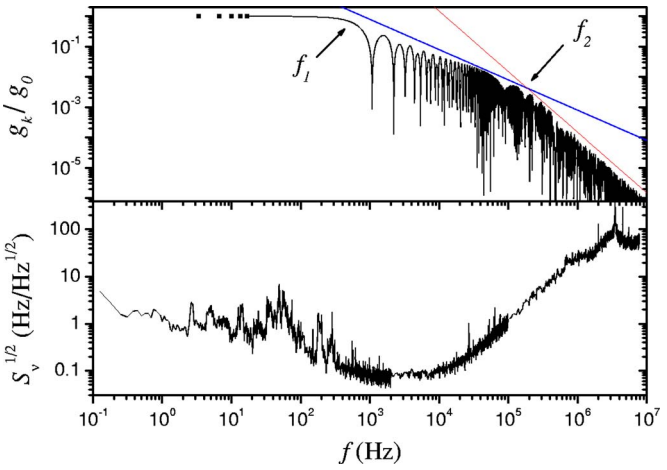

FIG. 13. (Color online) Fourier expansion of the sensitivity function and amplitude spectral density of the interrogation laser's frequency noise. Fourier coefficients are plotted as separate points only for the low frequency. At higher frequencies only the line connecting the coefficients is plotted for clarity.

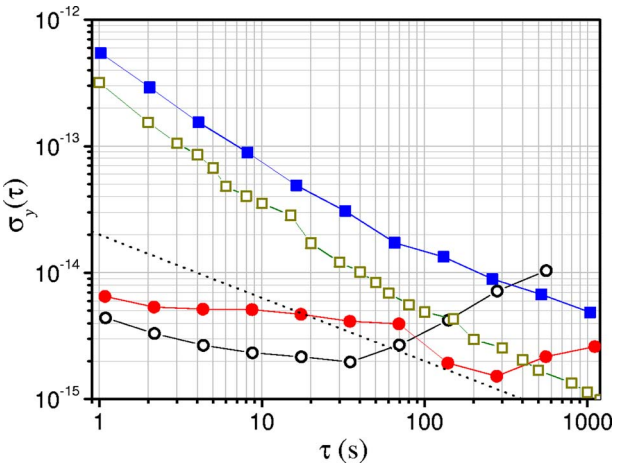

FIG. 14. (Color online) Relative Allan standard deviation of the frequency measurement (full squares). Open squares show the typical relative Allan standard deviation of the hydrogen maser. The stability of the Ca stabilized laser with respect to a cavity-stabilized laser with the linear drift of the resonator removed is shown by the full circles and the stability of two cavity-stabilized laser by the open circles. The calculated stability of the calcium standard of $\sigma_y(\tau)=2\times10^{-14}\,(\tau/\mathrm{s})^{-1/2}$ is indicated by the dashed line.

therefore the mean value is slightly larger than the estimated noise detailed above (see Table II). We attribute the excess noise to fluctuations in the trap position and temperature from shot to shot that lead to fluctuations in the single-pulse excitation probability when averaged over the atomic ensemble that are not normalized by the detection scheme.

In a different measurement session, the total noise of the measured excitation probability P_k at the point of steepest slope of the fringe was measured as

$$\mathcal{N}_{\mathrm{slope}}^2 = \frac{1}{N}\sum_{i=0}^{N-1}(P_{i+1}-P_i)^2 \tag{35}$$

to remove long term drift of the laser and measure only the uncorrelated noise between successive interrogations. We found a total noise of $\mathcal{N}_{\mathrm{slope}}=1\times10^{-2}$, that would lead to a relative frequency stability of $\sigma_{y,\mathrm{slope}}(1\ \mathrm{s})=7.3\times10^{-14}$ at 1 s averaging time. The difference to the stability expected from the Dick effect is probably caused by day-to-day variations of the performance of the interrogation laser and the parameters of the MOT. Table II sums up the contributions to the signal-to-noise ratio and to the frequency stability of the Ca frequency standard.

TABLE II. Noise and equivalent frequency stability contributions.

i	Contribution	$\mathcal{N}_i$	$\sigma_{y,i}(1\mathrm{s})$
1	QPN	8.3×10^{-5}	6×10^{-16}
2	PSN	2.6×10^{-5}	2×10^{-16}
3	Electronic	9×10^{-5}	7×10^{-16}
4	Detection laser	1.4×10^{-3}	1×10^{-14}
	Quad. sum 1–4	1.4×10^{-3}	1×10^{-14}
	Top and bottom fringe	4×10^{-3}	3×10^{-14}
5	Dick effect	2.7×10^{-3}	2×10^{-14}
	Quad. sum 1–5	3.0×10^{-3}	2×10^{-14}
	Slope of fringe	1×10^{-2}	7×10^{-14}

C. Measured frequency stability

The stability of the frequency reading during the frequency measurement is shown in Fig. 14. The reference during the averaging times of this measurement is a 100 MHz signal that is derived from the hydrogen maser of PTB [58]. We attribute the increased noise of the frequency measurement to excess noise of the femtosecond Ti:sapphire laser system [48,59–61] that was employed in this frequency comparison.

The stability for short times can also be inferred from a comparison between the Ca-stabilized laser and a laser that is stabilized to a second ultrastable resonator with the linear frequency drift of the resonator is removed (see Sec. III A). For times above the attack time of the lock to calcium and below times where the fluctuations of the drift of the resonator prevail ($\approx$300 s), the stability is close to $\sigma_y(\tau)=2\times10^{-14}\,(\tau/\mathrm{s})^{-1/2}$ in agreement with the estimated noise.

VII. CONCLUSIONS AND OUTLOOK

An optical frequency standard based on ultracold calcium atoms was realized. The frequency of the intercombination transition at 657 nm was measured with respect to the primary standard of time, the caesium clock, using a femtosecond comb generator. The total relative uncertainty was reduced to 1.2×10^{-14} limited by blackbody radiation of the calcium oven. Phase excursions in the spectroscopy pulses were quantitatively analyzed and corrected for.

In the near future, the uncertainty of the shift due to the blackbody radiation of the oven will be eliminated by deflecting atoms that were cooled with the Zeeman slower technique into the MOT. We expect to reduce the influence of the phase excursions during the excitation pulses by at least a factor of three by using AOM frequencies that lead to small frequency shifts. The frequency shift due to the linear Doppler effect mainly results from the relatively long delay time between the end of the atom interferometry and the first blue detection pulse of 800 μs. By improving the time sequence of the mechanical choppers and shutters this time can be reduced to 200 μs. With this the contribution of the linear Doppler effect can be reduced to 0.6 Hz. The total uncertainty would add up to 0.8 Hz corresponding to a relative total uncertainty of 2×10^{-15} close to the uncertainty of the best present caesium fountain clocks.

To further improve the frequency stability technical noise of the detection needs to be avoided and the Dick effect has to be reduced by, e.g., faster repetition of the interrogations and further reduction of frequency fluctuations of the interrogation laser. Then a unique quantum-projection limited frequency stability below 10^{-15} at one second averaging time seems reachable.

ACKNOWLEDGMENTS

This work was supported by the Deutsche Forschungsgemeinschaft (DFG) and by the European Union through the Human Potential program Cold Atoms and Ultra-precise Atomic Clocks (CAUAC). We thank R. Wynands and S. Weyers for help with the frequency measurement and E. Göbel for continuous support and the loan of the Ti:sapphire laser.

APPENDIX: LINEWIDTH OF THE CLOCK TRANSITION

Although the frequency of the clock transition is known with an uncertainty of a few Hertz only, the lifetime τ_c and thus the linewidth $\delta\nu=(2\pi\tau_c)^{-1}$ of the $4s4p\ ^3P_1$ state was not very well known. Values from the literature vary between 482 Hz and 279 Hz [62–64] and depend strongly on the experimental method that was used. Here, the linewidth was determined experimentally using an ensemble of ultracold Ca atoms. Ensembles of 2×10^6 to 4×10^7 atoms at a temperature of 15 μK were excited by a π pulse at 657 nm. The emitted fluorescence photons were detected with a photomultiplier tube and counted. A multichannel counter was used to bin the counts according to their arrival time. Due to the low velocity of the ultracold atoms they do not leave the detection region during the time of photon counting.

The following possible sources of systematic errors were checked. Saturation of the photomultiplier was not observed.

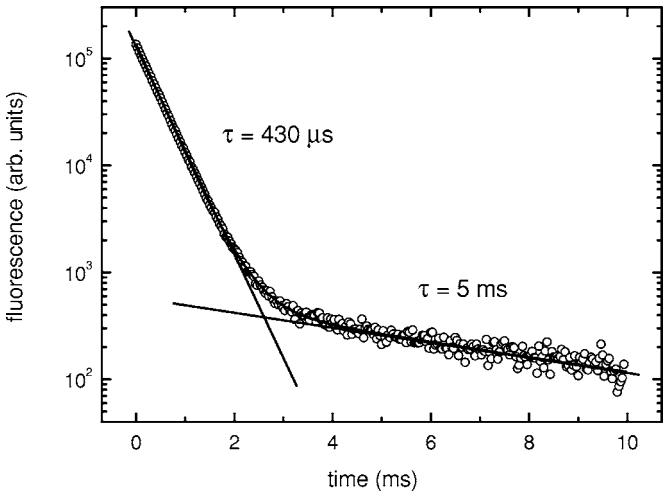

FIG. 15. Fluorescence of the intercombination transition after excitation with a π pulse. Fitting a double exponential curve to twelve data sets results in a time constant of (430 ± 10) μs. The second exponential decay is due to atoms accumulated in the $3d4s\ ^1D_2$ state during the MOT operation and decaying via the $4s4p\ ^3P_1$ state while detecting the fluorescence.

In a dense atomic ensemble reabsorption can mimic a longer lifetime. However, measurements at atomic densities between 8×10^8 cm^{-3} and 2×10^{10} cm^{-3} did not show systematic variations of the lifetime. The quench-laser beam was blocked during the time of fluorescence counting to avoid a shortening of the lifetime due to stray light. The background of detected photons without exciting the atoms by a π pulse was recorded and subtracted but it did not show any influence on the determined lifetime. Figure 15 shows an example of the recorded fluorescence signal. A double exponential decay was fitted to twelve data sets taken at different atomic densities resulting in lifetimes of the fast decay between 423 μs and 434 μs.

There was a slight dependency of the fitted lifetime on the count rate on the order of one percent. A linear extrapolation to zero count rate yields a lifetime of 425 μs of the $4s4p^3P_1$ state. According to the scatter in the data, an uncertainty of the lifetime of 10 μs is assumed, resulting in a natural linewidth of $\Delta\nu=(374\pm9)$ Hz.

The second decay constant has a much bigger value of a few milliseconds. Due to the small number of counted photons there is substantial scatter in the time constant between 2 ms and 7 ms when fitting the double exponential decay to the twelve data sets. The order of magnitude is consistent with the 3.3 ms lifetime for the decay of the $3d4s\ ^1D_2$ state into the $4s4p\ ^3P_1$ state [63]. Population in this state is due to an incomplete repumping from the $3d4s\ ^1D_2$ level during the cooling cycle in the second stage MOT.

[1] H. G. Dehmelt, IEEE Trans. Instrum. Meas. **IM-31**, 83 (1982).
[2] A. A. Madej and J. E. Bernard, in *Frequency Measurement and Control*, edited by A. N. Luiten, Topics in Applied Physics, Vol. 79 (Springer, Berlin, Heidelberg, New York, 2001), pp. 153–194.
[3] U. Sterr, C. Degenhardt, H. Stoehr, C. Lisdat, H. Schnatz, J. Helmcke, F. Riehle, G. Wilpers, C. Oates, and L. Hollberg, C. R. Phys. **5**, 845 (2004).
[4] S. T. Cundiff and J. Ye, Rev. Mod. Phys. **75**, 325 (2003).
[5] T. Udem, S. A. Diddams, K. R. Vogel, C. W. Oates, E. A. Curtis, W. D. Lee, W. M. Itano, R. E. Drullinger, J. C. Bergquist, and L. Hollberg, Phys. Rev. Lett. **86**, 4996 (2001).
[6] J. Helmcke, G. Wilpers, T. Binnewies, C. Degenhardt, U. Sterr, H. Schnatz, and F. Riehle, IEEE Trans. Instrum. Meas. **52**, 250 (2003).
[7] M. Takamoto, F.-L. Hong, R. Higashi, and H. Katori, Nature (London) **435**, 321 (2005).
[8] J. von Zanthier, T. Becker, M. Eichenseer, A. Y. Nevsky, C. Schwedes, E. Peik, H. Walther, R. Holzwarth, J. Reichert, T. Udem, T. W. Hänsch, P. V. Pokasov, M. N. Skvortsov, and S. N. Bagayev, Opt. Lett. **25**, 1729 (2000).
[9] J. Stenger, C. Tamm, N. Haverkamp, S. Weyers, and H. R. Telle, Opt. Lett. **26**, 1589 (2001).
[10] H. S. Margolis, G. P. Barwood, G. Huang, H. A. Klein, S. N. Lea, K. Szymaniec, and P. Gill, Science **306**, 1355 (2004).
[11] B. P. Anderson and M. A. Kasevich, Phys. Rev. A **50**, R3581 (1994).
[12] N. Beverini, F. Giammanco, E. Maccioni, F. Strumia, and G. Vissani, J. Opt. Soc. Am. B **6**, 2188 (1989).
[13] T. Binnewies, G. Wilpers, U. Sterr, F. Riehle, J. Helmcke, T. E. Mehlstäubler, E. M. Rasel, and W. Ertmer, Phys. Rev. Lett. **87**, 123002 (2001).
[14] K. Singer, S. Jochim, M. Mudrich, A. Mosk, and M. Weidemüller, Rev. Sci. Instrum. **73**, 4402 (2002).
[15] R. W. P. Drever, J. L. Hall, F. V. Kowalski, J. Hough, G. M. Ford, A. J. Munley, and H. Ward, Appl. Phys. B: Photophys. Laser Chem. **31**, 97 (1983).
[16] J. Ye, J.-L. Peng, R. J. Jones, K. W. Holman, J. L. Hall, D. J. Jones, S. A. Diddams, J. Kitching, S. Bize, J. C. Bergquist, L. W. Hollberg, L. Robertsson, and L. –S. Ma, J. Opt. Soc. Am. B **20**, 1459 (2003).
[17] C. J. Bordé, Phys. Lett. A **140**, 10 (1989).
[18] G. Wilpers, T. Binnewies, C. Degenhardt, U. Sterr, J. Helmcke, and F. Riehle, Phys. Rev. Lett. **89**, 230801 (2002).
[19] C. J. Bordé, C. Salomon, S. Avrillier, A. Van Lerberghe, C. Bréant, D. Bassi, and G. Scoles, Phys. Rev. A **30**, 1836 (1984).
[20] L. Allen and J. H. Eberly, *Optical Resonance and Two-Level Atoms* (Dover Publications Inc., New York, 1987).
[21] J. Vanier and C. Audoin, *The Quantum Physics of Atomic Frequency Standards* (Adam Hilger, Bristol and Philadelphia, 1989).
[22] T. Trebst, T. Binnewies, J. Helmcke, and F. Riehle, IEEE Trans. Instrum. Meas. **50**, 535 (2001).
[23] G. Wilpers, C. Degenhardt, T. Binnewies, A. Chernyshov, F. Riehle, J. Helmcke, and U. Sterr, Appl. Phys. B: Lasers Opt. **76**, 149 (2003).
[24] C. W. Oates, G. Wilpers, and L. Hollberg, Phys. Rev. A **71**, 023404 (2005).
[25] J. Hu, E. Ikonen, and K. Riski, Opt. Commun. **120**, 65 (1995).
[26] T. Trebst, PTB-Bericht PTB-Opt-60, Physikalisch-Technische Bundesanstalt, Braunschweig 1999.
[27] C. Degenhardt, H. Stoehr, U. Sterr, F. Riehle, and C. Lisdat, Phys. Rev. A **70**, 023414 (2004).
[28] F. Riehle, C. Degenhardt, C. Lisdat, G. Wilpers, H. Schnatz, T. Binnewies, H. Stoehr, and U. Sterr, in *Astrophysics, Clocks and Fundamental Constants*, edited by S. G. Karshenboim and E. Peik, Lecture Notes in Physics, Vol. 648 (Springer, Berlin, Heidelberg, New York, 2004), pp. 229–244.
[29] GUM, *Guide to the expression of uncertainty in measurement*, ISO/TAG 4. Published by ISO, 1993 (corrected and reprinted, 1995) in the name of the BIPM, IEC, IFCC, ISO, UPAC, IUPAP and OIML (1995), ISBN number: 92-67-10188-9, 1995.
[30] C. Degenhardt, T. Nazarova, C. Lisdat, H. Stoehr, U. Sterr, and F. Riehle, IEEE Trans. Instrum. Meas. **54**, 771 (2005).
[31] S. Weyers, U. Hübner, R. Schröder, C. Tamm, and A. Bauch, Metrologia **38**, 343 (2001).
[32] F. Pereira Dos Santos, H. Marion, S. Bize, Y. Sortais, A. Clairon, and C. Salomon, Phys. Rev. Lett. **89**, 233004 (2002).
[33] T. Ido, T. H. Loftus, M. M. Boyd, A. D. Ludlow, K. W. Holman, and J. Ye, Phys. Rev. Lett. **94**, 153001 (2005).
[34] N. Beverini and F. Strumia, in *Interaction of Radiation with Matter, A Volume in honour of A. Gozzini* (Quaderni della Scuola Normale Superiore de Pisa, Pisa, 1987), pp. 361–373.
[35] G. Zinner, PTB-Bericht PTB-Opt-58, Physikalisch-Technische Bundesanstalt, Braunschweig, 1998.
[36] C. W. Oates, F. Bondu, R. W. Fox, and L. Hollberg, Eur. Phys. J. D **7**, 449 (1999).
[37] K. Zeiske, PTB-Bericht PTB-Opt-48, Physikalisch-Technische Bundesanstalt, Braunschweig, 1995.
[38] R. Grimm, M. Weidemüller, and Y. B. Ovchinnikov, Adv. At., Mol., Opt. Phys. **42**, 95 (2000).
[39] A. R. Edmonds, *Angular Momentum in Quantum Mechanics* (Princeton University Press, Princeton, NJ, 1957).
[40] R. L. Kurucz and B. Bell, Atomic line data, Kurucz CD-ROM No. 23, Cambridge MA.: Smithsonian Astrophysical Observatory, 1995, URL http://cfa-www.harvard.edu/amdata/ampdata/kurucz23/sekur.html, typing error of $A(4s5s\ ^3S-4s4p\ ^3P)$ has been corrected from the original data.
[41] H. Bethe and E. Salpeter, in *Handbuch der Physik*, edited by S. Flügge (Springer, Berlin, 1957), Vol. XXXV.
[42] G. von Oppen, Z. Phys. **227**, 473 (1970).
[43] J. W. Farley and W. H. Wing, Phys. Rev. A **23**, 2397 (1981).
[44] J. Li and W. A. van Wijngaarden, Phys. Rev. A **53**, 604 (1996).
[45] F. Riehle, J. Ishikawa, and J. Helmcke, Phys. Rev. Lett. **61**, 2092 (1988).
[46] T. Kurosu and A. Morinaga, Phys. Rev. A **45**, 4799 (1992).
[47] H. Schnatz, B. Lipphardt, J. Helmcke, F. Riehle, and G. Zinner, Phys. Rev. Lett. **76**, 18 (1996).
[48] J. Stenger, T. Binnewies, G. Wilpers, F. Riehle, H. R. Telle, J. K. Ranka, R. S. Windeler, and A. J. Stentz, Phys. Rev. A **63**, 021802(R) (2001).
[49] G. Wilpers, C. W. Oates, S. A. Diddams, A. Bartels, W. H. Oskay, J. C. Bergquist, and L. Hollberg, "Ultra-high stability optical frequency standard based on laser-cooled neutral calcium," Conference contribution CWJ4, CLEO QELS 2005, Baltimore, USA, 2005.
[50] D. W. Allan, Proc. IEEE **54**, 221 (1966).
[51] C. Audoin and B. Guinot, *The Measurement of Time: Time, Frequency and the Atomic Clock* (Cambridge University Press,

Cambridge, UK, New York, 2001).
[52] G. Santarelli, P. Laurent, P. Lemonde, A. Clairon, A. G. Mann, S. Chang, A. N. Luiten, and C. Salomon, Phys. Rev. Lett. **82**, 4619 (1999).
[53] W. M. Itano, J. C. Bergquist, J. J. Bollinger, J. M. Gilligan, D. J. Heinzen, F. L. Moore, M. G. Raizen, and D. J. Wineland, Phys. Rev. A **47**, 3554 (1993).
[54] G. J. Dick, in *Proceedings of 19th Annual Precise Time and Time Interval (PTTI) Applications and Planning Meeting*, Redondo Beach, CA, 1987 (U. S. Naval Observatory, 1988), pp. 133–147.
[55] G. J. Dick, J. D. Prestage, C. A. Greenhall, and L. Maleki, in *Proceedings of the 22nd Annual Precise Time and Time Interval (PTTI) Applications and Planning Meeting, Vienna, VA*, 1990 (NASA, CP-3116) pp. 487–509.
[56] A. Quessada, R. P. Kovacich, I. Courtillot, A. Clairon, G. Santarelli, and P. Lemonde, J. Opt. B: Quantum Semiclassical Opt. **5**, S150 (2003).
[57] P. Lemonde, G. Santarelli, P. Laurent, F. P. D. Santos, A. Clairon, and C. Salomon, in *Proceedings of Frequency Control Symposium* (IEEE, Piscataway, NJ, 1998), p. 110.
[58] A. Bauch and S. Weyers, Phys. Rev. D **65**, 081101(R) (2002).
[59] H. R. Telle, B. Lipphardt, and J. Stenger, Appl. Phys. B: Lasers Opt. **74**, 1 (2002).
[60] H. R. Telle and U. Sterr, in *Frequency Measurement and Control: Advanced Techniques and Future Trends*, edited by A. N. Luiten (Springer, Berlin, Heidelberg, New York, 2001), pp. 295–313.
[61] J. Stenger and H. R. Telle, in *Proceedings of SPIE: Laser Frequency Stabilization, Standards, Measurement and Applications*, edited by J. L. Hall and J. Ye (Bellingham, WA, 2001), Vol. 4269, pp. 72–76.
[62] P. G. Whitkop and J. R. Wiesenfeld, Chem. Phys. Lett. **69**, 457 (1980).
[63] R. Drozdowski, J. Kwela, and M. Walkiewicz, Z. Phys. D: At., Mol. Clusters **27**, 321 (1993).
[64] R. Drozdowski, M. Ignaciuk, J. Kwela, and J. Heldt, Z. Phys. D: At., Mol. Clusters **41**, 125 (1997).